rsif.royalsocietypublishing.org

Research

Article submitted to journal

Keywords:
bio-medical robotics, soft actuators, dielectric elastomer actuators, dynamic modeling, neuroprosthetics

Author for correspondence:
Corresponding author
e-mail: yves.perriard@epfl.ch

Dynamic modeling for the control of reinforced dielectric elastomer actuators for post-paralysis facial movement restoration.

Stefania Konstantinidi[1,2], Ning Liu[3], Raki Ben Mustapha[1,2], Simon Holzer[1,2], Markus Koenigsdorff[1,2], Amine Benouhiba[1,2], Yoan Civet[1,2], Yves Perriard[1,2]

[1] Ecole polytechnique fédérale de Lausanne (EPFL), Integrated Actuators Laboratory (LAI), Neuchâtel, Switzerland
[1] Ecole polytechnique fédérale de Lausanne (EPFL), Center for Artificial Muscles (CAM), Neuchâtel, Switzerland
[3] Université de Franche-Comté, SUPMICROTECH, CNRS, institut FEMTO-ST, F-25000 Besançon, France

Dielectric Elastomer Actuators (DEAs) stand out as versatile devices with promising applications. Their use has been proposed as artificial muscle implants, aiming to replace paralyzed facial muscles and restore the corresponding movements. By reinforcing DEAs with unidirectional fibers, substantial uni-axial deformations can be induced, resulting in previously reported strains up to 75% higher than isotropic DEAs. In this work, the control of the actuator is explored by investigating the dynamic electro-viscoelastic response of a dielectric elastomers with transversally isotropic properties. A model for anisotropic viscoelastic dielectric elastomers is proposed, which is employed to describe the actuator's dynamic response and design a closed loop controller in order to achieve a precise actuation of the facial prosthesis. The model is validated with two types of input signals. The control system demonstrated its efficacy in minimizing error and improving actuation performance. The designed prosthesis showed a RMSE of 2.06% in response to electromyography signals recording movement on the zygomaticus major muscle responsible for smiling.

THE ROYAL SOCIETY PUBLISHING

1. Introduction

The design of artificial muscles capable of mimicking the behavior of natural muscles has become an important focus in soft robotics and prosthetic development. Several actuation methods have been developed for this purpose, ranging from pneumatic and thermal systems to electroactive approaches [1]. An emerging alternative for facial reanimation is the application of artificial muscles, which provide a less invasive route to recovering natural movement following paralysis [2, 3]. Facial paralysis is a challenging condition [4] which can be treated surgically in case of chronic paralysis [5]. By replacing the two-stage free muscle transfer approach, artificial muscles may simplify treatment and enable patients to achieve recovery more rapidly. Facial muscle activity is governed by neural input from the facial nerves. Clinically, crossover nerve transfer is a common treatment for paralysis and can similarly provide control signals for artificial muscle prostheses [6]. This approach involves transferring neural activity from the unaffected side of the face to the paralyzed side, thereby restoring coordinated and symmetric movement.

Recent progress in the field of soft actuators, namely artificial muscles, has led to the development of soft implantable devices aiming to replace paralyzed muscles and restore lost function [3]. Such implants rely on the use of Dielectric Elastomer Actuators (DEAs) [7]. DEAs produce deformation when subjected to an electric field [8]. They operate as deformable capacitors composed of a soft dielectric membrane sandwiched between flexible electrodes. Upon voltage application, electrostatic forces compress the membrane's thickness and induce significant lateral expansion [9]. However, the control of DEAs is challenging notably due to their non-linear deformations, their viscoelasticity and hysteresis, as well as the electromechanical instabilities. Feedforward controllers have been demonstrated by Zou et al. [10], as well as by Gupta et al. [11]. The latter presented a dynamic, nonlinear and viscoelastic model to predict the actuator responses and design a feedforward control scheme for replicating jaw motions. Liu et al. [12] proposed a control-focused model capable of capturing instabilities, including the snap-through phenomenon in multi-layered tubular DEAs for cardiac support [13]. Beyond model-based approaches, feedback mechanisms and learning-based control strategies, such as reinforcement learning, have been applied to improve DEA performance [14, 15].

In this work, we focus on the dynamic behavior of uniaxial anisotropic fiber-reinforced DEAs (uFRDEAs) to achieve significant uniaxial deformations for applications such as medical implants and artificial muscles. By limiting deformation along the fiber direction, the actuators can be more precisely controlled. Inspired by the structure of biological tissues and muscles [16], fiber reinforcement introduces anisotropic behavior, where material properties vary with direction, similar to that observed in natural systems. Incorporating fibers into DEAs helps directing their motion, minimize necking, and enhance overall performance, including strain capacity, stress handling, and frequency response. In this work, a dynamic model for reinforced DEAs is introduced to study the stability and design of a controller for such actuators. Compared to existing static models of anisotropic fiber-reinforced DEAs [7, 17], dynamic models consider both the time-dimension and the viscoelastic properties of the actuator to describe the resulting oscillations. Adding fibers to the DEAs presents advantages for the dynamic control, as they decrease the visco-elastic behavior, thus increasing force, response speed and strain. Existing dynamic models of DEAs include distributed parameter models, formulated with partial differential equations (PDEs), and lumped parameter models. While distributed parameter models offer precise dynamic simulation, they pose challenges in numerical simulation and controller implementation due to PDE approximation. Contrarily, lumped parameter models simplify the DEA into segments with ordinary differential equations, facilitating simulation and controller design. A novel dynamic model for uFRDEAs is studied in this work dedicated to facial reanimation. This modeling is necessary for controller design in order to achieve precise actuation of the facial prosthesis in real-time.

The paper is organized as follows: In Section II, the problem statement is described. The main metrics, physics and governing equations of electro-mechanical transduction of DEAs are given to establish a dynamic non-linear transversely isotropic model of the actuator. Section III describes the state-space representation of the uFRDEA, along with the unknown parameters' identification of the established model. The simulated and experimental results are used to implement a closed loop PID controller which is described in Section IV. Finally, Section V and VI conclude the article and present the perspectives of the proposed work.

2. Dynamic modeling of transversely isotropic DEAs

In this work, the dynamic behavior of uFRDEAs is investigated. As shown in Fig. 1a), when a time-dependent voltage $V_{in}(t) = V_{in}$ is applied on the thickness z-direction, an expansion occurs in the in-plane x- and y-directions. When the DEA is constrained in one direction, the displacement in the perpendicular direction is enhanced as in Fig. 1b). The uFRDEAs consist of an elastomer matrix layer, denoted with the index m, and a fiber layer, denoted with the index f. The initial dimensions are defined as l_{m0}, l_{f0}, w_{m0}, w_{f0} and t_{m0}, t_{f0} for the length, width and thickness of the matrix and fibers respectively. $l_m(t)$, $l_f(t)$ denotes the length, $w_m(t)$, $w_f(t)$ the width, $t_i(t)$, $t_f(t)$ the thickness of the fibers and matrix respectively at time t, and n_f the number of fibers, which remains constant throughout time.

royalsocietypublishing.org/journal/rsif J R Soc Interface Focus 0000000

The stretch ratios of the membrane are then defined as:

$$\lambda_x(t) = \frac{w_m(t)}{w_{m0}}, \tag{2.1}$$

$$\lambda_y(t) = \frac{l_m(t)}{l_{m0}}, \tag{2.2}$$

$$\lambda_z(t) = \frac{t_m(t)}{t_{m0}}. \tag{2.3}$$

The actuator is assumed to be incompressible and satisfies the condition $\lambda_x(t)\lambda_y(t)\lambda_z(t) = 1$, resulting in:

$$\lambda_z(t) = \frac{1}{\lambda_x(t)\lambda_y(t)}. \tag{2.4}$$

The electric dynamics of DEA can be represented as in Fig. 2 by a non-linear capacitance C_{DEA} which is in parallel with a non-linear resistance R_d, both of which are in series with a resistance R_a representing the resistance of the contact points of the DEA (surface resistance of the electrodes and connections). R_a is assumed to remain constant throughout actuation. C_{DEA} and R_d will change with the deformation of the DEA, such as :

$$C_{DEA}(t) = \epsilon_r \epsilon_0 \frac{A_{m0}\lambda_x(t)^2\lambda_y(t)^2}{t_{m0}}, \tag{2.5}$$

$$R_d(t) = \rho \frac{t_{m0}}{A_{m0}\lambda_x(t)^2\lambda_y(t)^2}. \tag{2.6}$$

where ϵ_r and ϵ_0 represent the material's relative permittivity and the vacuum permittivity, respectively. ρ denotes the material resistivity, $A_{m0} = l_{m0}w_{m0}$ denotes the initial in-plane surface of the DEA surface. According to Kirchoff's voltage law, the following equation is established:

$$V_{in} = V_{in}(t) = R_a i(t) - V_{DEA}(t) \tag{2.7}$$

The DEA will thus charge at a voltage:

$$V_{DEA} = V_{DEA}(t) = V_{in} e^{\frac{-t}{R_d C_{DEA}}} \tag{2.8}$$

When voltage V_{in} is applied between the electrodes, the electric field produces a pressure onto the dielectric matrix. This electro-mechanical stress, namely the Maxwell stress is given by:

$$\sigma_\epsilon = -\epsilon_r \epsilon_0 E^2, \tag{2.9}$$

where E denotes the electric field such as $E = \frac{V_{DEA}}{t_m}$.

For the mechanical transduction, a rheological representation is used considering the Generalized Maxwell model (Fig. 2). Spring-damper elements in parallel represent the viscoelastic stress σ_v. The Maxwell stress coupled with the material transversely isotropic hyperelastic stress are described as non-linear springs. The resulting stress σ_{DEA} is written as:

$$\sigma_{DEA} = \sigma_m + \sigma_v. \tag{2.10}$$

The constitutive behavior of a DEA can be expressed as in [9] for $i = x, y, z$:

$$\sigma_{m,i} = \lambda_i \frac{\partial W(\mathbf{C}, \tilde{E})}{\partial \lambda_i}. \tag{2.11}$$

The total strain energy density W of the system consists of two parts: a mechanical contribution W_s and a electrical contribution W_E, such as :

$$W(\mathbf{C}, \tilde{E}) = W_s(\mathbf{C}) + W_E(\mathbf{C}, \tilde{E}). \tag{2.12}$$

Here, $\mathbf{C}$ denotes the Cauchy–Green deformation tensor, which characterizes the material's deformation state.

W_E can be written as:

$$W_E(\lambda_x, \lambda_y, \tilde{E}) = -\frac{\epsilon_0 \epsilon_r}{2} \tilde{E}^2 (\lambda_x \lambda_y)^2. \tag{2.13}$$

The uFRDEAs exhibit transverse isotropy, and their strain energy is formulated as a function of the first three invariants of the Cauchy–Green deformation tensor, together with two additional quasi-invariants [18, 19] that describe the influence of fiber orientation. These fiber-related terms are defined using a unit direction vector, denoted $\mathbf{a_0}$. The strain energy can be separated further into two components: the total strain energy of the system, W_{iso}, and the contribution from the

royalsocietypublishing.org/journal/rsif J R Soc Interface Focus 0000000

anisotropic reinforcement with the fibers, W_{aniso}. The volume fractions of the matrix and fibers are denoted v_m and v_f respectively. The mechanical strain energy can then be expressed as a function of the invariants I_1 to I_5:

$$W_s = W_s(I_1, I_2, I_3, I_4, I_5) \tag{2.14}$$

$$W_s = v_m \cdot W_{iso}(I_1, I_2, I_3) + v_f \cdot W_{aniso}(I_4, I_5). \tag{2.15}$$

The isotropic matrix energy W_{iso} can be represented using the Yeoh model:

$$W_{iso}(I_1, I_2, I_3) = W_{iso}(I_1) = \sum_{i=3}^{3} C_{i0}(I_1 - 3)^i. \tag{2.16}$$

where the mechanical parameters C_{i0} are determined from uniaxial testing under the relevant boundary conditions. For uni-axial fibers, where $\mathbf{a_0} = [1\ 0\ 0]$ the quasi invariants are written as $I_4 = \lambda_x^2$ and $I_5 = \lambda_x^4$.

The fibers are considered to exhibit linear elastic behavior, meaning their stress–strain response follows a linear relationship characterized by a Young's modulus E_f. The anisotropic strain energy component W_{aniso} is defined accordingly as [17]:

$$W_{aniso}(I_4, I_5) = W_{aniso}(I_4) = \frac{(\sqrt{I_4} - 1)^2 \cdot E_f}{2}. \tag{2.17}$$

Therefore, the coupled anisotropic hyper-elastic and Maxwell stress along the y-axis is written as:

$$\sigma_m = v_m \lambda_y \frac{\partial W_{iso}(\lambda_x, \lambda_y)}{\partial \lambda_y} + v_f \lambda_y \frac{\partial W_{aniso}(\lambda_x, \lambda_y)}{\partial \lambda_y} - \epsilon_0 \epsilon_r \tilde{E} \lambda_y \lambda_x^2. \tag{2.18}$$

The visco-elastic stress is defined as:

$$\sigma_v = \sum_{i}^{N} k_{vi}(\varepsilon_1(y) - \varepsilon_{\eta i}) + \eta_{v0} \frac{\partial \varepsilon_1(y)}{\partial y} v, \tag{2.19}$$

where $v = \dot{y} = \frac{dy}{dt}$ is the velocity, $\varepsilon_1(y) = \lambda_y - 1$ is the strain along the y-axis and $\varepsilon_{\eta i}$ are internal strains.
The resulting coupled electro-mechanical force F_{DEA} along the y-axis is given by:

$$F_{DEA}(t) = F_{DEA} = (\sigma_m + \sigma_v)A, \tag{2.20}$$

where $A = l_m \lambda_y w_m \lambda_x$ is the cross section of the uFRDEA.

3. State modelling of the fiber-reinforced actuator

According to Fig. 3, the equation of motion of the DEA can be written as:

$$m l_{m0} \frac{d^2 \lambda_y}{dt^2} = F_{DEA} - F_s. \tag{3.1}$$

In the case of smiling, a load F_s, defined by the facial tissues assimilated to a spring of stiffness constant k, is attached in the y direction, thus acting as a pre-load. The pre-load related to facial tissues is adapted to the mean stiffness of 22.4 kPa/mm which is determined by performing measurements on facial tissues located at the cheek [20]. Among different metrics evaluated in the study, these reported values are considered for the determination of a tissue surrogate and thus taken into account for the actuator modeling and setup design.

By choosing the state variables as follows:

$$x = (x_1 \quad x_2 \quad x_3 \quad \dots \quad x_{i+2})^T \tag{3.2}$$

$$x = (\lambda_y \quad \dot{\lambda_y} \quad \sigma_{v1} \quad \dots \quad \sigma_{vi})^T \tag{3.3}$$

and substituting the previous Eqs. into Eq. 3.1, the state space representation of the DEA dynamics is formulated as:

$$\dot{x}_1 = x_2, \tag{3.4}$$

$$\dot{x}_2 = -\frac{1}{m l_{m0}}(F_{DEA} - F_s) \tag{3.5}$$

$$\dot{x}_3 = k_{v1}(\frac{d\lambda_y}{dx_1})x_2 - \frac{k_{v1}}{\eta_1}x_3 \tag{3.6}$$

$$\dot{x}_{i+2} = k_{vi}(\frac{d\lambda_y}{dx_1})x_2 - \frac{k_{vi}}{\eta_1}x_{i+2} \tag{3.7}$$

The system is non-linear such as:

royalsocietypublishing.org/journal/rsif J R Soc Interface Focus 0000000

$$\dot{x}_1 = f_1(x_1, x_2, x_3, x_4), \tag{3.8}$$

$$\dot{x}_2 = f_2(x_1, x_2, x_3, x_4), \tag{3.9}$$

$$\dot{x}_3 = f_2(x_1, x_2, x_3, x_4), \tag{3.10}$$

$$\dot{x}_4 = f_2(x_1, x_2, x_3, x_4). \tag{3.11}$$

$$\dot{x} = f(x, u), \tag{3.12}$$

where u is the applied voltage. The mechanical parameters of the actuators are determined with uni-axial tensile tests and the viscoelastic parameters of the model are determined with a step response evaluation. The identification process is carried out with the nonlinear graybox in System Identification toolbox of Matlab. The identification method is chosen to be 'lsqnonlin', and the solver is 'ode45'. The evaluation of the parameters leads to a step-response model accuracy of 76.7 % as shown in Figure 4.

Table 1. Identified parameter values

Parameter		Value	Unit
Yeoh's coefficient	C_{10}	213	kPa
Yeoh's coefficient	C_{20}	-182	kPa
Yeoh's coefficient	C_{30}	155	kPa
Damping	η_0	155	kPa.s
Damping	η_1	20	kPa.s
Damping	η_2	19	kPa.s
Stiffness	k_1	2.7	MPa
Stiffness	k_2	3	MPa

The system dynamics are analyzed at the equilibrium configuration, corresponding to the state in which the DEA stabilizes under a constant applied mechanical load. At this point, the system is linearized and the Jacobian J of the system takes the form:

$$J = \begin{pmatrix} \frac{\partial f_1}{\partial x_1} & \frac{\partial f_1}{\partial x_2} & \frac{\partial f_1}{\partial x_3} & \frac{\partial f_1}{\partial x_4} \\ \frac{\partial f_2}{\partial x_1} & \frac{\partial f_2}{\partial x_2} & \frac{\partial f_2}{\partial x_3} & \frac{\partial f_2}{\partial x_4} \\ \frac{\partial f_3}{\partial x_1} & \frac{\partial f_3}{\partial x_2} & \frac{\partial f_3}{\partial x_3} & \frac{\partial f_3}{\partial x_4} \\ \frac{\partial f_4}{\partial x_1} & \frac{\partial f_4}{\partial x_2} & \frac{\partial f_4}{\partial x_3} & \frac{\partial f_4}{\partial x_4} \end{pmatrix} \tag{3.13}$$

$$J = \begin{pmatrix} 0 & a_{12} & 0 & 0 \\ a_{21} & a_{22} & a_{23} & a_{24} \\ 0 & a_{32} & a_{33} & 0 \\ 0 & a_{42} & 0 & a_{44} \end{pmatrix} = A|_{eq} \tag{3.14}$$

and

$$\begin{pmatrix} \frac{\partial f_1}{\partial u} \\ \frac{\partial f_2}{\partial u} \\ \frac{\partial f_3}{\partial u} \\ \frac{\partial f_4}{\partial u} \end{pmatrix} = \begin{pmatrix} b_1 \\ b_2 \\ 0 \\ 0 \end{pmatrix} = B|_{eq} \tag{3.15}$$

The linearized state space model is therefore:

$$\dot{x} = Ax + Bu \tag{3.16}$$

Finally, the transfer function of the system can be established with the form:

$$G(s) = \frac{\alpha s^2 + \beta s + \gamma}{s^4 + \delta s^3 + \zeta s^2 + \theta s + \iota} \tag{3.17}$$

Where α, β,..., ι are determined by solving the model. The final transfer function according to the actuator properties and boundary conditions is used to tune the controller.

4. Actuator control

(a) Setup and characterization

An anatomically precise setup is proposed integrating the prosthesis for smiling movement as illustrated in Figure 5. In this study, silicone is used as a skin and muscle surrogate due to its ability to simulate a wide range of skin properties, its ease of manipulation, non-toxicity, long-term stability, and durability, making it ideal for replicating the complex biomechanical behavior of human tissues [21, 22].

The design of the boundary tissues is laser cut (Trotec Speedy 360®) to fabricate a mold in PMMA. The liquid silicone is prepared by mixing two parts of LSR4305 (Elkem) and poured into the mold. It is then put in a vacuum chamber for 4 hours in order to remove any residual air bubbles and cured for 2 hours at 80°C before being unmolded. The skull is drilled where the muscles should be attached, and the silicone is mounted on the skull. The silicone tissue is characterized mechanically by attaching a clip at the DEA position and pulling from the rest position. The model is then used to design the DEA according to the biasing characteristics of the fabricated silicone tissues. An optimization loop is considered and the resulting fiber reinforced DEA dimensions are of 300 µm thickness and 20 mm width. The DEAs are fabricated with two active silicone layers of 100 µm each, (Elastosil 2030® from Wacker Chemie), carbon-based electrodes (mixture of conductive carbon black (EC-600J), isopropanol, and liquid silicone rubber (LSR 4305, Wacker Chemie)) [23] and reinforced with 100 µm thick PET fibers. The fibers are glued with silicone, which acts as a final encapsulation layer. The in-plane dimensions of the DEA are 20 mm x 50 mm.

The movement of facial muscles is is driven by neural impulses carried along the facial nerves, and a comparable strategy involves actuating the prosthesis through a neural interface placed on the healthy hemiface, enabling control of the DEA positioned on the paralyzed side. The actuation of DEAs has been demonstrated in previous work with an open loop using electromyography (EMG) signals in real time [3]. Although the signals qualitatively match, there is a significant difference in the amplitudes of the actuation signal and the monitored DEA displacement, reaching 40 % errors. To overcome this limitation, a closed loop control of the actuator is proposed in this work.

(b) Closed loop control

A closed loop control system is used to adjust the actuator's displacement with real-time feedback. A laser displacement sensor (Keyence LK-G3) is positioned to continuously monitor the displacement of the DEA, which is attached to the surrogate tissue on the skull setup. The feedback provided by the sensor is used to adjust the voltage applied to the DEA, ensuring that the desired displacement is achieved and maintained. A PID controller adjusts the input voltage based on the displacement error of the DEA, where the objective is to achieve accurate displacement control. The standard formulation of a PID controller is expressed as:

$$C(s) = K_p + \frac{K_i}{s} + K_d s \tag{4.1}$$

where K_p, K_i, and K_d are the proportional (P), integral (I), and derivative (D) gains, respectively. The proportional term adjusts the output based on the magnitude of the error, the integral term helps eliminating steady-state error by considering the accumulation of past errors, and the derivative component helps reduce overshoot by responding to the rate of change of the error. In order to design the PID controller, the open-loop transfer function is first derived by combining the transfer function $G(s)$ with the controller $C(s)$:

$$T(s) = C(s)G(s) \tag{4.2}$$

This transfer function is used to adjust the PID gains, with the objective of minimizing the steady-state error, achieving a fast response without overshoot, and ensuring system stability.

As described in the diagram of Figure 6, in the closed-loop system, the PID controller then adjusts the input voltage $V_{in}(s)$ according to the error signal, defined as the difference between the target displacement $R(s)$ and the actual displacement $Y(s)$, measured by the laser displacement sensor. The control law is given by:

$$V_{in}(s) = C(s)E(s) = C(s)[R(s) - Y(s)] \tag{4.3}$$

where $E(s)$ represents the error signal. The actuator dynamics and feedback control loop work together to reduce the error, ensuring that the actual displacement $Y(s)$ closely follows the desired displacement $R(s)$. The PID controller is implemented in Simulink and adjustments to K_p, K_i, and K_d are made iteratively. Real-time feedback from the laser sensor ensures that the input voltage to the DEA is dynamically adjusted to minimize the error between the nominal and actual displacement.

EMG signals are considered for the actuation, where the applied EMG surface electrodes were recording the zygomaticus major muscle in a healthy person while pronouncing the word "hello" (/hE'l@/).

The results as well as the error between the actuation signal and the measured displacement are illustrated in Figure 7. It can be seen that the implementation of a closed-loop control system significantly enhanced the accuracy of the DEA's

actuation. The root mean square error (RMSE) between the reference command and the measured displacement was used to quantify performance: for the open-loop actuation is of 4.42 %, whereas with a closed loop control this error drops to a RMSE of 2.06 %. This error is deemed acceptable for the proposed application as sub-millimeter movements are not considered visible. The errors are regrouped in Table 2.

5. Discussion and perspectives

The dynamic model developed for the uFRDEAs successfully captures the electro-mechanical interactions, providing an accurate description of the actuator's time-dependent response with an accuracy to a step response higher than 75 %. Through the state-space model, a PID controller was designed and tested, demonstrating the effectiveness of closed-loop control in achieving stable and precise actuation. The controller compensates for non-linearities and viscoelastic delays, ensuring real-time adjustments for facial reanimation applications. With a reduction of the RMSE from 4.42% in the open-loop system to 2.06% in the closed-loop system, the control system demonstrated its effectiveness in minimizing error and improving actuation performance. Introducing dynamic modeling of fiber reinforced DEAs presents advantages for the control, as reinforced actuators decrease the visco-elastic behavior, thus increasing force, response speed and strain. Apart from the proposed application for facial movement restoration, notably smiling, the proposed model can be employed for various applications in robotics and prosthetic implants. Alternative control models for improved performance can also be explored such as with neural networks. For the final application, the integration of alternative sensors that are more compatible with human integration should be considered. Rather than relying on external devices, such as laser-based displacement measurement, the DEA's self-sensing capabilities can be used [24, 25]. Future work should also focus on disturbances of the system due to the boundary load variations when the person moves.

6. Conclusion

This work introduces a non-linear anisotropic dynamic model for uFRDEAs, specifically tailored for use in artificial muscles for facial movement restoration. The model accounts for the anisotropic and viscoelastic properties of the actuators and provides a foundation for the design of a controller. The experimental and simulated results confirm the feasibility of using these actuators for facial prosthesis applications, offering a faster recovery option for patients suffering from facial paralysis. Future work may explore more complex control strategies and real-time implementations to enhance performance in practical biomedical and robotics applications.

Data Accessibility. All data are available in the main text or the supplementary materials.

Competing Interests. The authors declare no competing interests.

Funding. This project is graciously supported by the Werner Siemens-Stiftung.

References

[1]W. Liang, H. Liu, K. Wang, Z. Qian, L. Ren, and L. Ren, "Comparative study of robotic artificial actuators and biological muscle", Advances in Mechanical Engineering **12**, 168781402093340 (2020).
[2]S. Konstantinidi, T. Martinez, A. Benouhiba, Y. Civet, and Y. Perriard, "Soft Actuators for Facial Reanimation", in 2022 IEEE/RSJ International Conference on Intelligent Robots and Systems (IROS) (2022), pages 11109–11114.
[3]S. Konstantinidi, C. Imholz, T. Martinez, A. Benouhiba, A. Walter, Y. Civet, N. Lindenblatt, and Y. Perriard, "Real-time actuation of a dielectric elastomer actuator neuroprosthesis for facial paralysis", Smart Materials in Medicine **5** (2023).
[4]J. Nellis et al., "Association among facial paralysis, depression, and quality of life in facial plastic surgery patients", JAMA facial plastic surgery **19**, 190–196 (2017).
[5]J. Chan et al., "Management of Facial Paralysis in the 21st Century", Facial plastic surgery : FPS **27**, 346–57 (2011).
[6]N. Yoshioka and J. Fernandez-Miranda, "Nerve to the zygomaticus major muscle: An anatomical study and surgical application to smile reconstruction", Clinical Anatomy **37** (2023).
[7]T. Lu, J. Huang, C. Jordi, G. Kovacs, R. Huang, D. Clarke, and Z. Suo, "Dielectric elastomer actuators under equal-biaxial forces, uniaxial forces, and uniaxial constraint of stiff fibers", Soft Matter **8**, 6167– (2012).
[8]Y. Bar-Cohen, "Electroactive Polymers as Artificial Muscles: A Review", Journal of Spacecraft and Rockets **39**, 822–827 (2002).
[9]Z. Suo, "Theory of dielectric elastomers", en, Acta Mechanica Solida Sinica **23**, 549–578 (2010).
[10]J. Zou and G. Gu, "Feedforward control of the rate-dependent viscoelastic hysteresis nonlinearity in dielectric elastomer actuators", IEEE Robotics and Automation Letters **4**, 2340–2347 (2019).
[11]U. Gupta, Y. Wang, H. Ren, and J. Zhu, "Dynamic modeling and feedforward control of jaw movements driven by viscoelastic artificial muscles", IEEE/ASME transactions on mechatronics **24**, 25–35 (2018).
[12]N. Liu, T. Martinez, A. Walter, Y. Civet, and Y. Perriard, "Control-oriented modeling and analysis of tubular dielectric elastomer actuators dedicated to cardiac assist devices", IEEE Robotics and Automation Letters **7**, 4361–4367 (2022).

[13]T. Martinez, S. E. Jahren, A. Walter, J. Chavanne, F. Clavica, L. Ferrari, P. P. Heinisch, D. Casoni, A. Haeberlin, M. M. Luedi, et al., "A novel soft cardiac assist device based on a dielectric elastomer augmented aorta: An in vivo study", Bioengineering & translational medicine **8**, e10396 (2023).

[14]T. Yang et al., "A soft artificial muscle driven robot with reinforcement learning", Scientific Reports **8**, 10.1038/s41598-018-32757-9 (2018).

[15]L. Li, J. Li, L. Qin, J. Cao, M. Kankanhalli, and J. Zhu, "Deep Reinforcement Learning in Soft Viscoelastic Actuator of Dielectric Elastomer", IEEE Robotics and Automation Letters **PP**, 1–1 (2019).

[16]L. Liu, C. Zhang, L. Meng, X. Chen, D. Li, and H. Chen, "A biologically inspired artificial muscle based on fiber-reinforced and electropneumatic dielectric elastomers", Smart Materials and Structures **26** (2017).

[17]S. Konstantinidi, T. Martinez, B. Tandon, Y. Civet, and Y. Perriard, "Uni-axial reinforced dielectric elastomer actuators with embedded 3D printed fibers", Smart Materials and Structures **32** (2023).

[18]L. Brown and L. Smith, "A Simple Transversely Isotropic Hyperelastic Constitutive Model Suitable for Finite Element Analysis of Fiber Reinforced Elastomers", Journal of Engineering Materials and Technology **133**, 021021 (2011).

[19]J. Weiss, B. Marker, and S. Govindjee, "Finite element implementation of incompressible, isotropic hyperelasticity transversely", Comput. Methods Appl. Mech. Eng. **135**, 108–128 (1996).

[20]M. Beatty, A. Wee, D. Marx, L. Ridgway, B. Simetich, T. Sousa, K. Vakilzadian, and J. Schulte, "Viscoelastic Properties of Human Facial Skin and Comparisons with Facial Prosthetic Elastomers", Materials **16**, 2023 (2023).

[21]L. LIN, J. Li, and X. ZENG, "The Development of Physical Skin Model for Biomechanical Applications", Journal of the Society of Biomechanisms **41**, 129–136 (2017).

[22]A. Piątek, G.-M. Rotaru, S. Derler, F. Spano, M. Camenzind, S. Annaheim, R. Stämpfli, M. Schmid, and R. Rossi, "Materials used to simulate physical properties of human skin", Skin Research and Technology **22**, 3–14 (2016).

[23]S. Holzer, A. Walter, S. Konstantinidi, T. Martinez, Y. Civet, and Y. Perriard, "Carbon based printed electrodes for DEAs: study of pad, inkjet, and stencil printing", in Electroactive Polymer Actuators and Devices (EAPAD) XXVI, Vol. 12945, edited by J. D. W. Madden, S. S. Seelecke, and A. L. Skov (International Society for Optics and Photonics, 2024), 129450U.

[24]G. Rizzello, D. Naso, A. York, and S. Seelecke, "Closed Loop Control of Dielectric Elastomer Actuators Based on Self-Sensing Displacement Feedback", Smart Materials and Structures **25**, 035034 (2016).

[25]S. Rosset, B. O'Brien, T. Gisby, D. Xu, H. Shea, and I. Anderson, "Self-sensing dielectric elastomer actuators in closed-loop operation", Smart Materials and Structures **22**, 104018 (2013).

royalsocietypublishing.org/journal/rsif J R Soc Interface Focus 0000000

royalsocietypublishing.org/journal/rsif J R Soc Interface Focus 0000000

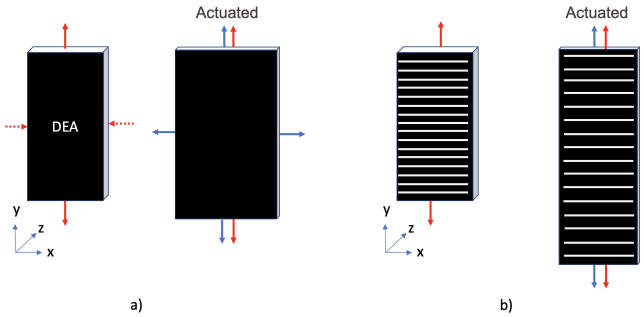

Figure 1. a) Illustration of a DEA exposed to uniaxial external forces (red) and its corresponding actuation state (blue). b) Behavior of a uniaxial anisotropic fiber-reinforced DEA under identical uniaxial forces, shown both at rest and when voltage is applied. The x-axis deformation is limited, whereas the y-axis experiences enhanced strain.

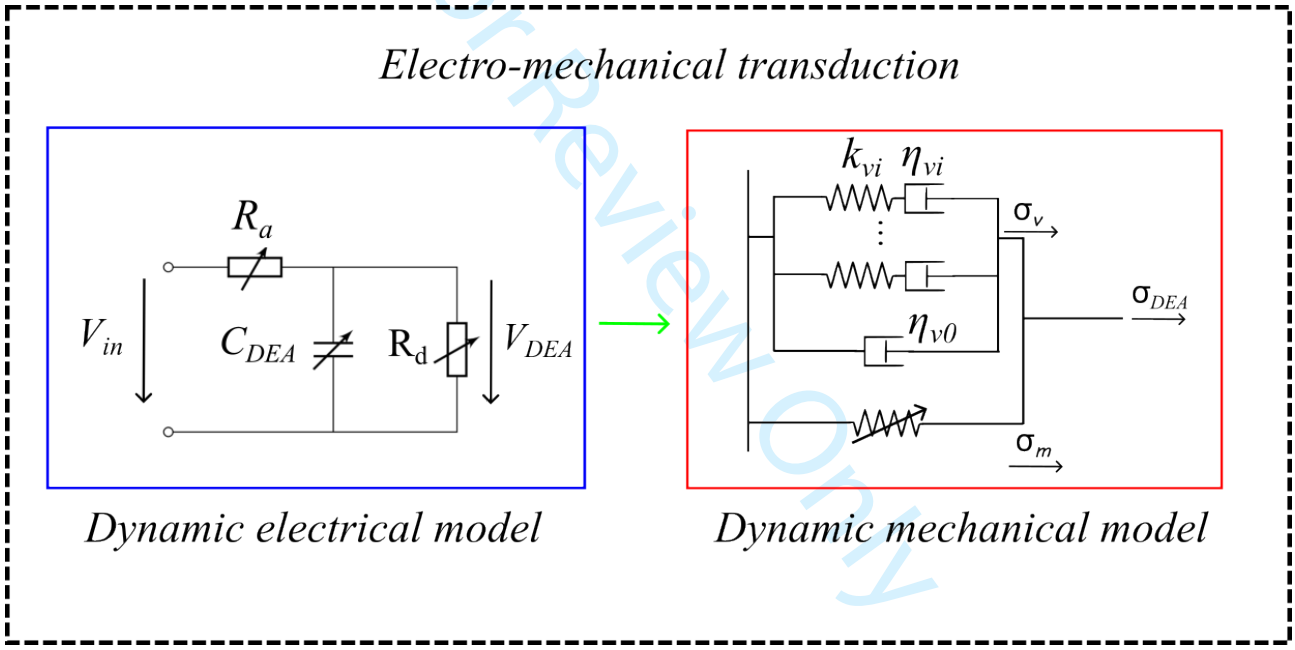

Figure 2. Schematics of the actuator dynamic electrical and mechanical models.

Table 2. Errors between the command signal and the measured displacement.

	RMSE [%]	STD	Min. error	Max. error
Open-loop	4.42	13.01	0.0139	41.21
Closed-loop	2.06	5.04	0.0012	21.88

royalsocietypublishing.org/journal/rsif J R Soc Interface Focus 0000000

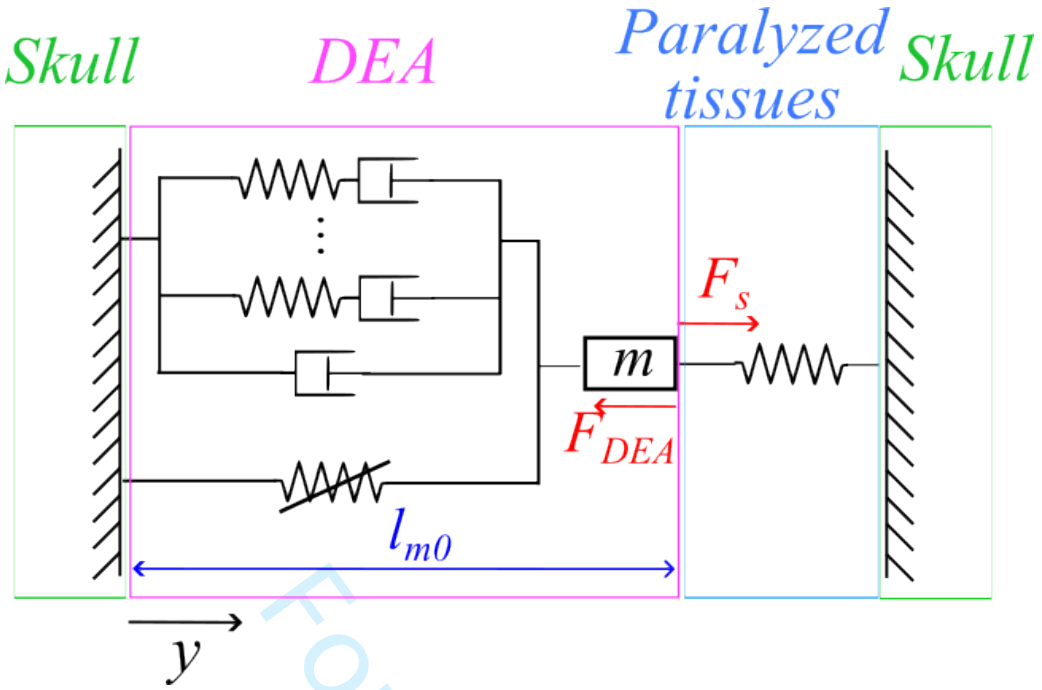

Figure 3. Schematics of the system geometry.

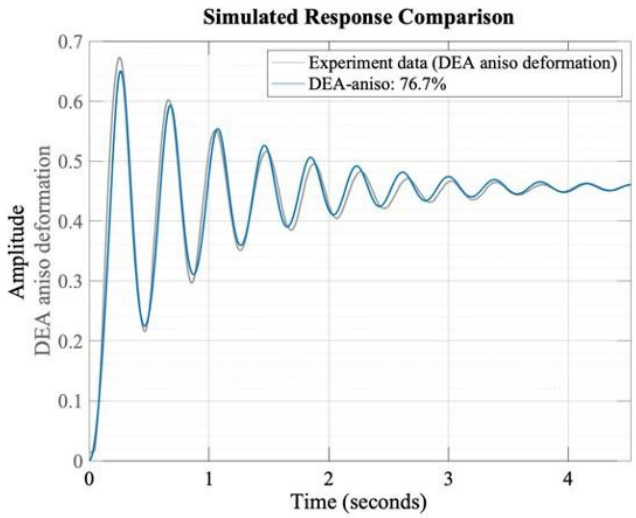

Figure 4. Comparison of the measurements with the modeled dynamic actuator response to a step input voltage with the identified parameters.

royalsocietypublishing.org/journal/rsif J R Soc Interface Focus 0000000

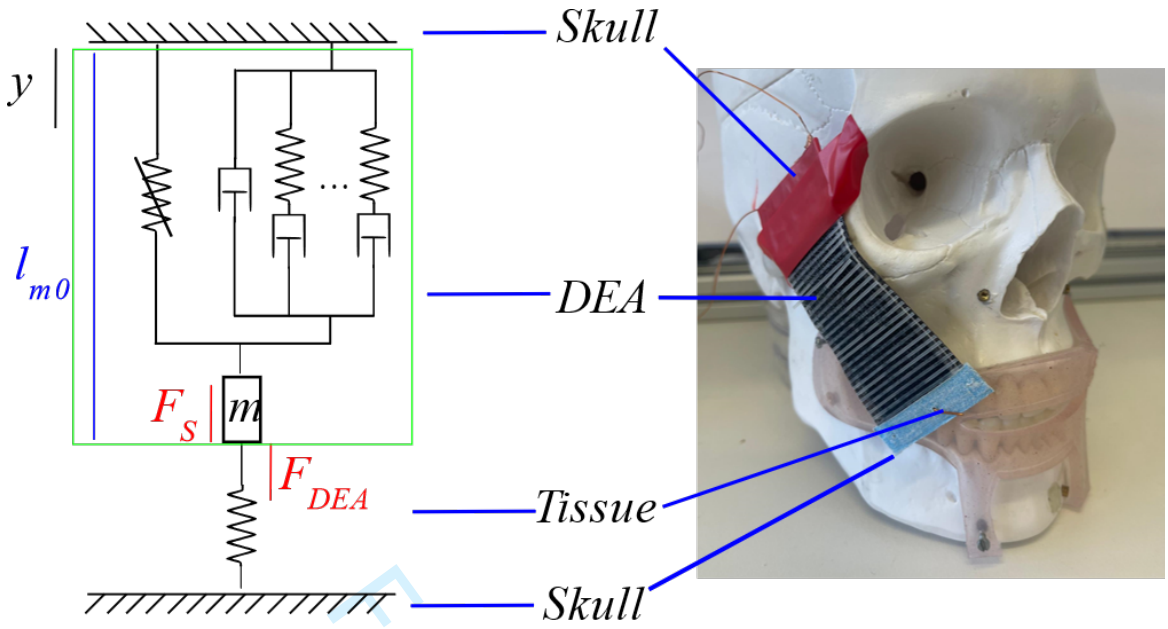

Figure 5. Illustration of the setup for the closed-loop actuation of the DEAs.

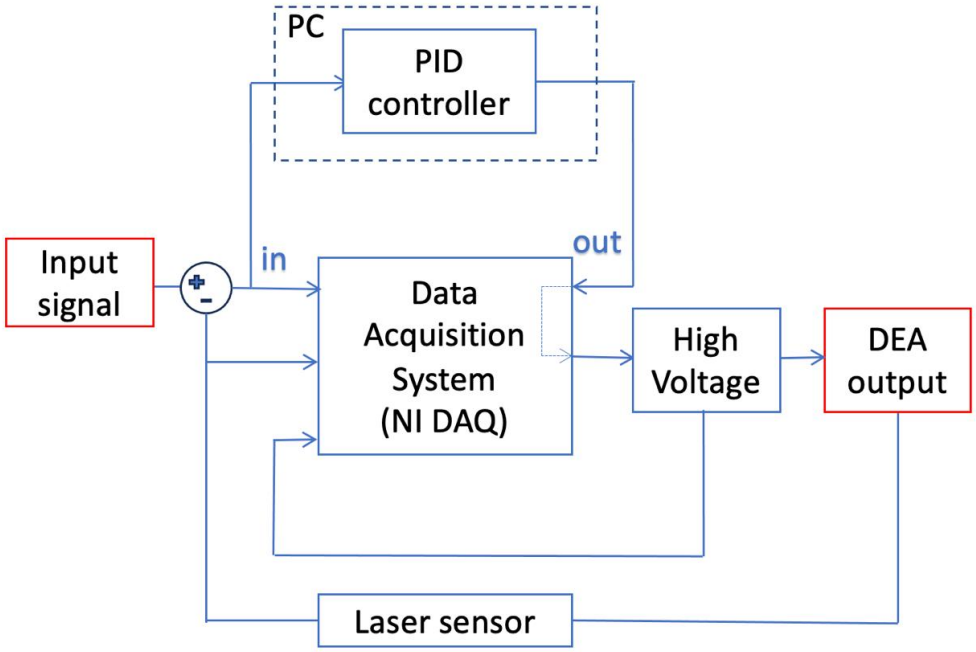

Figure 6. Schematics of the control diagram. A PID controller is implemented and a laser sensor is used for the feedback of the DEA displacement.